Proceedings of the 7th International Symposium on Cavitation
CAV2009
August 17-22, 2009, Ann Arbor, Michigan, USA

CAV2009 – Paper No. 142

High-speed photography of supercavitation and multiphase flows in water entry

Hong-Hui Shi
College of Mechanical Engineering & Automation,
Zhejiang Sci-Tech University,
Hangzhou 310018, Zhejiang Province, China

Motoyuki Itoh
Department of Mechanical Engineering,
Nagoya Institute of Technology,
Nagoya 466-8555, Aichi Prefecture, Japan

ABSTRACT

The supercavitation in water entry and associated multiphase flows were studied using a high-speed camera and single-shot optical device. The formation, growth and collapse of supercavities induced by underwater high-speed projectiles were revealed. The unsteady fluid dynamic processes of the splash, surface deformation, supercavity twisting, down jet in the cavity, etc. were also studied. Both axisymmetrical and three-dimensional supercavities were found in the experiment. The shape of the axisymmetrical supercavity has been compared with Logvinovich's model. The three-dimensional supercavity is caused by the trajectory deflection of the underwater projectile, which is also related unsteadiness and turbulence of the flow field. When the supercavity is twisted, a grain-like cavitating bubble is formed after the upper and lower pinch-offs. It is newly found that during the surface closure (surface seal), the down-jet is generated simultaneously with the formation of upwards splash dome.

1 INTRODUCTION

With the increasing demand of developing high-speed undersea weapons, the research on supercavitation induced by high-speed underwater bodies has been increased [1,2]. The requirement to thoroughly understand the flow field has motivated newly started fundamental research of water entry [3,4]. Hrubes [5] reported a flow visualization of high-subsonic and transonic supercavities when the projectile velocity was around the acoustic velocity of water 1500 m/s. From his experiment, it is understood that the contact of the cavity wall with the body surface may generate a lift force to cause trajectory deflection of the body. Klomfass and Salk [6] performed a numerical simulation of compressible supercavitating flows using a finite-volume method. The equations of state for liquid and gas were selected carefully in their simulation. Neaves and Edwards [7] presented a sophisticated computation program for supercavitating flows of underwater projectile in a wide velocity range from subsonic to supersonic. In their computation of water entry flow, the effect of non-condensing gas by air entrainment on the cavity closure was emphasized.

Savchenko [8-10] reviewed a nearly half century long systematic research on supercavitation in the former Soviet Union. The documents show that their work mainly experienced three steps: (1) establishment of theory, (2) dimensional analysis, (3) experimental validation. Vlasenko [11] reported three test facilities at the Institute of Hydromechanics, Ukrainian National Academy of Science, which are capable of producing 50-1300 m/s supercavities. Krischner [12] also introduced experimentation of generating ~1500 m/s supercavities at the Naval Undersea Warfare Center, USA. In this paper, we will present a continued effort to study supercavitation and some interesting phenomena have been revealed.

2 EXPERIMENTAL SET UP

The experimental set-up is shown in Fig. 1. A projectile vertically impacts into a water tank which is 0.6 m×0.6 m×0.8 m and is made from 5 mm thick stainless plates. The water tank has two windows at each side for optical observation. It was once considered to use a gas gun to accelerate the projectile. However, to accelerate a projectile up to a velocity of several hundred meters per second requires a long acceleration tube and high-pressure driving gas. As a result, a large amount of gases ahead and behind the projectile come out and these gases would disturb the water surface to bring about an unwanted supercavitation. Therefore, an Anschutz rifle (made in

Germany) was chosen to fire a 352 m/s projectile of 5.7 mm in diameter, 12.3 mm in total length and 2.67 g in mass. To prevent any effect of the muzzle shock wave and powder explosion gas on the water surface, a special designed porous exhaust silencer (blast diffuser) was fixed at the gun muzzle and the rifle was set a sufficient distance away from the water surface.

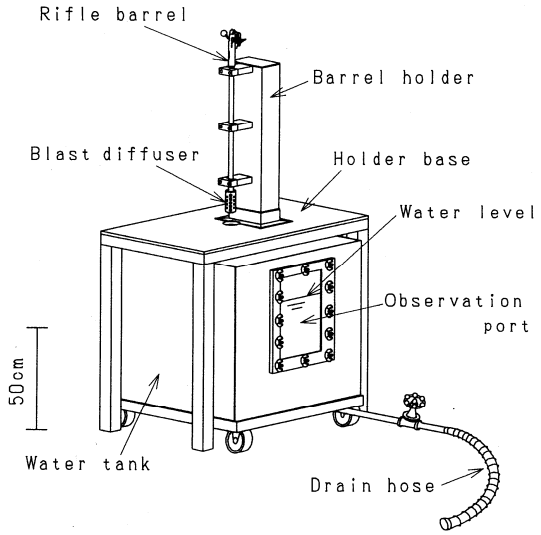

Figure 1: Supercavitation experiment set up

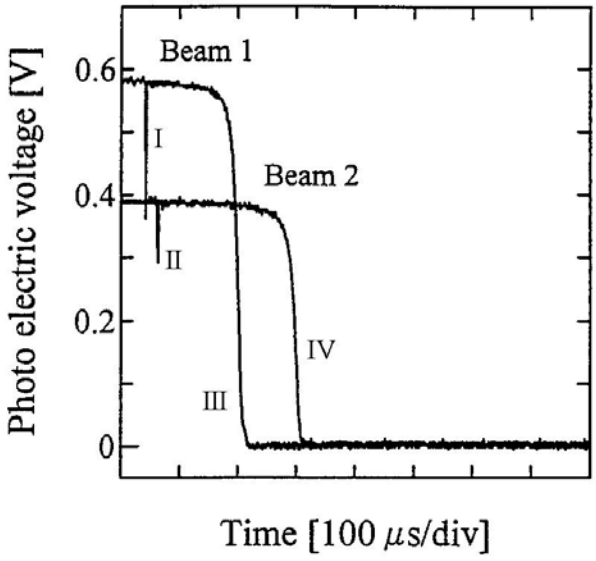

Figure 2: Velocity measurement of underwater projectile by the method of cutting laser beam. The first laser beam is 71 mm below the water surface and the second laser beam is 102 mm below the water surface

The projectile velocity in air and its change at different water depth were measured in detail by a method of cutting two laser beams [13]. When a projectile moves downwards across the laser beams, the photoelectric currents of the two photodiodes are shut off. Using a digital oscilloscope, the time interval between the photovoltage drops of the two photodiodes is measured and the velocity of the projectile is obtained. Figure 2 is a typical example. In the figure, signals I and II are caused by the underwater shock wave that is generated when the projectile impacts on the water surface [14-15]. Signals III and IV are caused when the projectile itself cross the laser beams. Therefore, the velocities of the underwater projectile and shock wave are calculated to be 329 m/s and 1476 m/s respectively. This demonstrates the measurement system has sufficient sensitivity and accuracy.

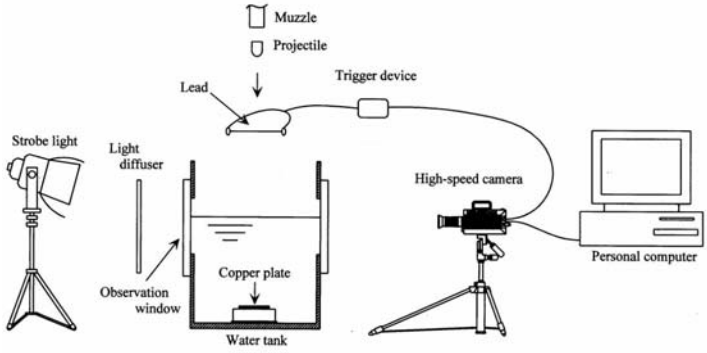

Figure 3: Schematic of the high-speed photographic system

The high-speed photography system has also been shown in Fig. 3. A digital high-speed video camera (Memrecam ci-4, Nac Co., Ltd.) was used, which can operate at 500, 1000 and 2000 fps framing rates respectively. The camera was triggered when a 0.5 mm diameter carbon rod, above the water surface, was broken by the impact of the projectile. The image signals taken by the camera were sent to a personal computer for processing. The light source was put at the other side of the water tank and a light diffuser was used to improve the illumination background. Using a xenon flash (NP-1A, 180 ns exposure time, Sugahara Laboratory), the single-shot of the sequence in water entry was photographed.

3 RESULTS AND DISCUSSIONS

3.1 Axisymmetric Supercavity

Figure 4 gives the sequences of an axisymmetric supercavitation. The interframe time is 0.5 ms. In Fig. 4(1), the projectile has penetrated into water and induced a supercavity. In Fig. 2(2), an upwards moving splash forms. This process has actually caused the surface closure of the cavity. Meanwhile, a thin down jet forms in the cavity. A thicker down jet is formed after the cavity is pulled away from the surface (Figs. 4(7)-(11)). In Figs. 4(14)-(16), the cavity begins to break up and collapse. The collapsed cavity has a helical shape, which will rebound and collapse again (Figs. 4(17)-(20)).

In Fig. 4(2), the height of the splash is almost same as the

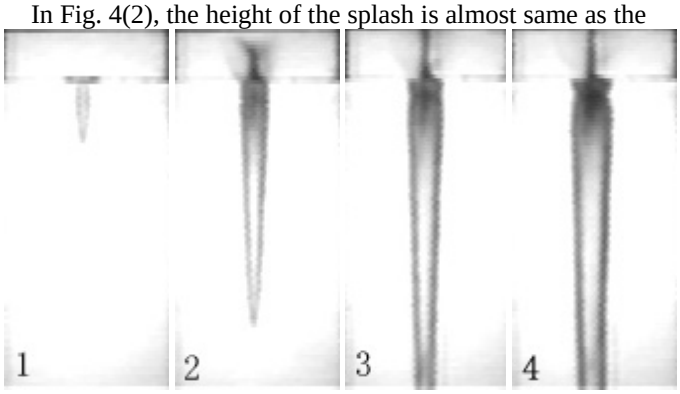

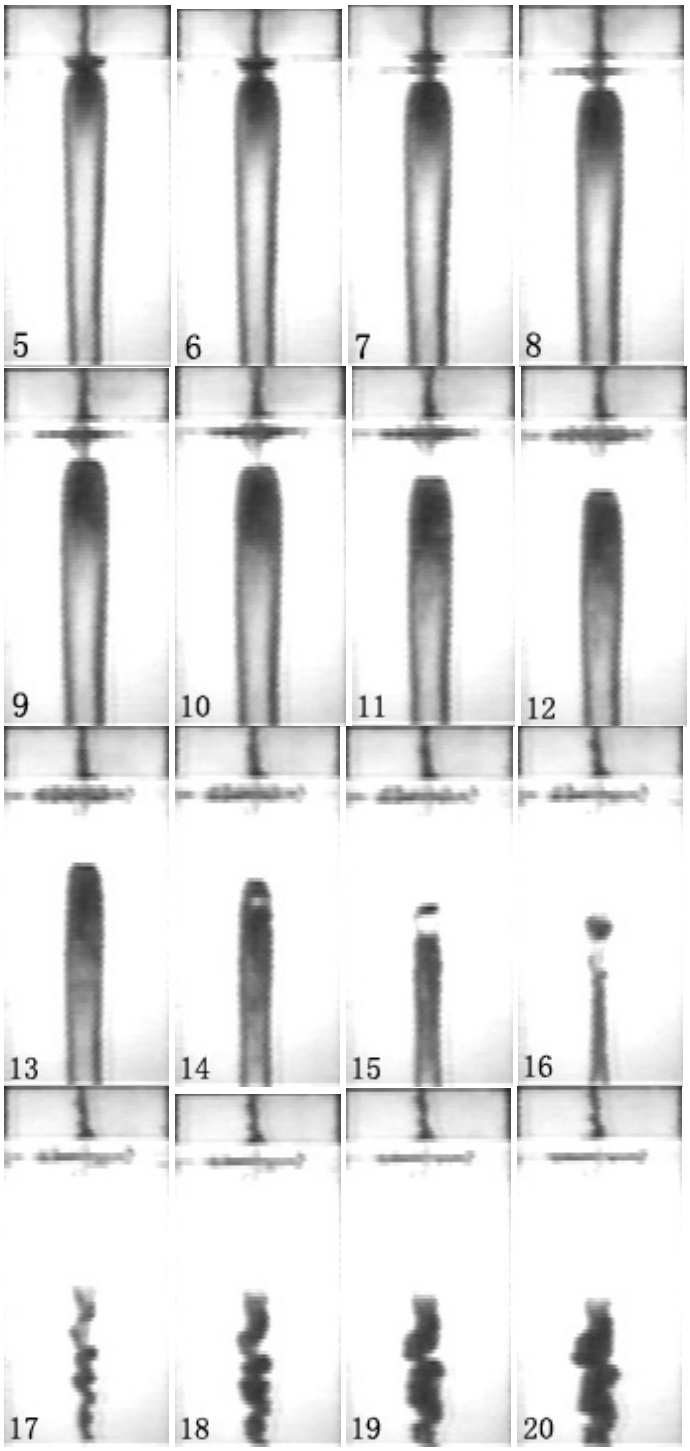

Figure 4: High-speed photographs of an axisymmetric supercavitation. The time between successive images is 0.5 ms. The height of each picture is 400 mm

length of the down jet beneath the water surface. From Fig. 4(1) to Fig. 4(2), the splash velocity is measured as $U_s \approx 84.21$ m/s. This value is in agreement with the previous measurement [15]. The down jet velocity U_j at the moment should be close to U_s. Once the supercavity is formed, its diameter gradually expands and reaches a maximum value in Fig. 4(7). Then the cavity is pulled away from the water surface. The averaging pulling velocity from Fig. 4(5) to Fig. 4(10) is measured as $U_p \approx 19.31$ m/s. From Fig. 4(14) to Fig. 4(16), the end section at the supercavity's top breaks up and forms a discrete bubble. However, the bubble later emerges again with the tail of the long helical shaped bubble in Fig. 4(17).

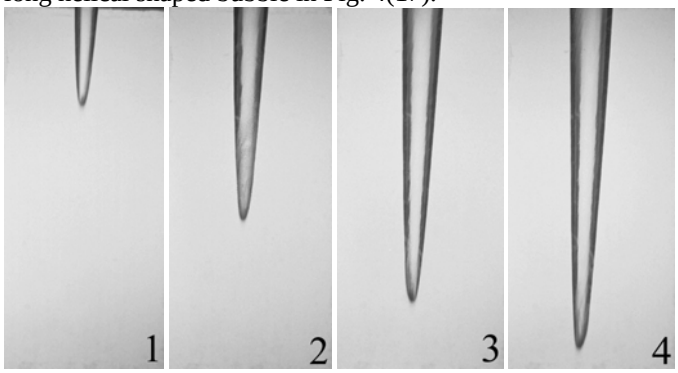

Figure 5: Single-shot photographs of axisymmetric supercavities at different water depth. The height of each picture is 400 mm. The top of the pictures is at 70 mm water depth

Figure 5 shows single-shot photographs of axisymmtric supercavities at different water depth. Combining Figs. 4 and 5, one can get that the maximum diameter and the total length of the supercavity are D_c = 54.15 mm and L_c = 430.77 mm respectively. The whole profile of the cavity is obtained by matching the cavity shape in Fig. 5 with that in Fig. 4 at the 70 mm water depth. In accordance with the semi-empirical theory of Logvinovich [8-10], D_c and L_c can be expressed as

$$D_c = D_n\sqrt{\frac{c_x}{k\sigma}}, L_c = \frac{D_n}{\sigma}\sqrt{c_x \ln\frac{1}{\sigma}} \quad (1)$$

$$c_x = c_{x0}(1+\sigma) \quad (2)$$

$$\sigma = \frac{p - p_c}{\frac{1}{2}\rho V^2} \quad (3)$$

where D_n is the diameter of cavitator, k = 0.9-1.0, c_x drag coefficient, c_{x0} drag coefficient without cavitation. σ is the cavitation number. In Eq. (3), V, ρ, p and p_c are projectile velocity, fluid density, fluid pressure and cavity pressure respectively. The cavity shape is described as [8-10]

$$\frac{D}{D_c} = \sqrt{1-\left(1-\frac{D_1^2}{D_c^2}\right)\left(1-\frac{2x}{L_c}\right)^2} \quad (4)$$

where $D_1 = 1.92D_n$. Equation (4) means the cavity diameter at coordinate x.

In case of natural cavitation, the saturation vapor pressure p_v may be used to replace the cavity pressure p_c. At 20°C water temperature, p_v is 2350 Pa [8]. The fluid pressure is

$$p = p_0 + \rho g Z \quad (5)$$

where p_0 is atmosphere, g gravity acceleration, Z water depth. The water depth in Fig. 5(4) has reached Z = 450 mm. The cavitation number σ is calculated to be 1.63×10^{-3}. In our experiment, the projectile has a parabolic front shape [16] so that according to Knapp et al. [17] we take c_{x0} = 0.2. It is also known that D_n = 5.7 mm. Then we rewrite Eq. (4) into

$$\frac{D}{D_n}=\frac{D_c}{D_n}\sqrt{1-\left(1-\frac{D_1^2}{D_c^2}\right)\left[1-2\left(\frac{L_c}{D_n}\right)^{-1}\frac{x}{D_n}\right]^2} \qquad (6)$$

Figure 6 has compared Eq. (6) with the experimental data of Figs. 4 and 5. The solid line in the figure is the theory and the triangles are the experimental data. It is seen that the discrepancy between the theory and the experiment is obvious.

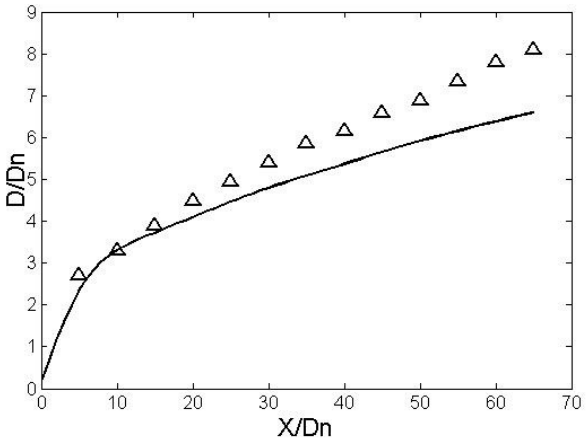

Figure 6: Comparison between the experimental data and Logvinovich's model of supercavity shape. The solid line is Eq. (6). The triangles are experimental data

3.2 Three-dimensional Supercavity

Figure 7 gives the sequences of a three-dimensional supercavitation. In Fig. 7(1), the cavity surface is still open and the air goes into the cavity at this stage. The projectile has penetrated 77.60 mm in water. From the empirical velocity attenuation formula of the projectile in water obtained by Shi and Takami [13,18], the projectile velocity at a water depth Z is described as

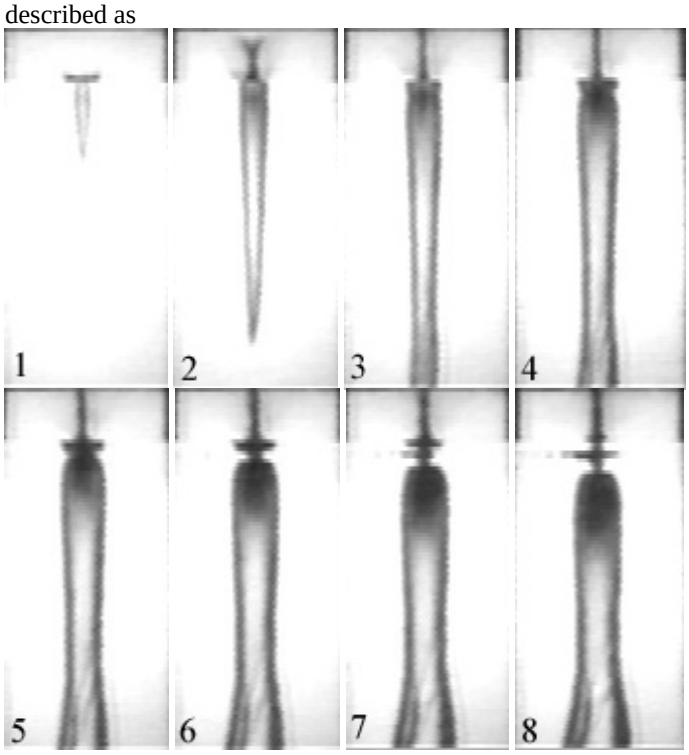

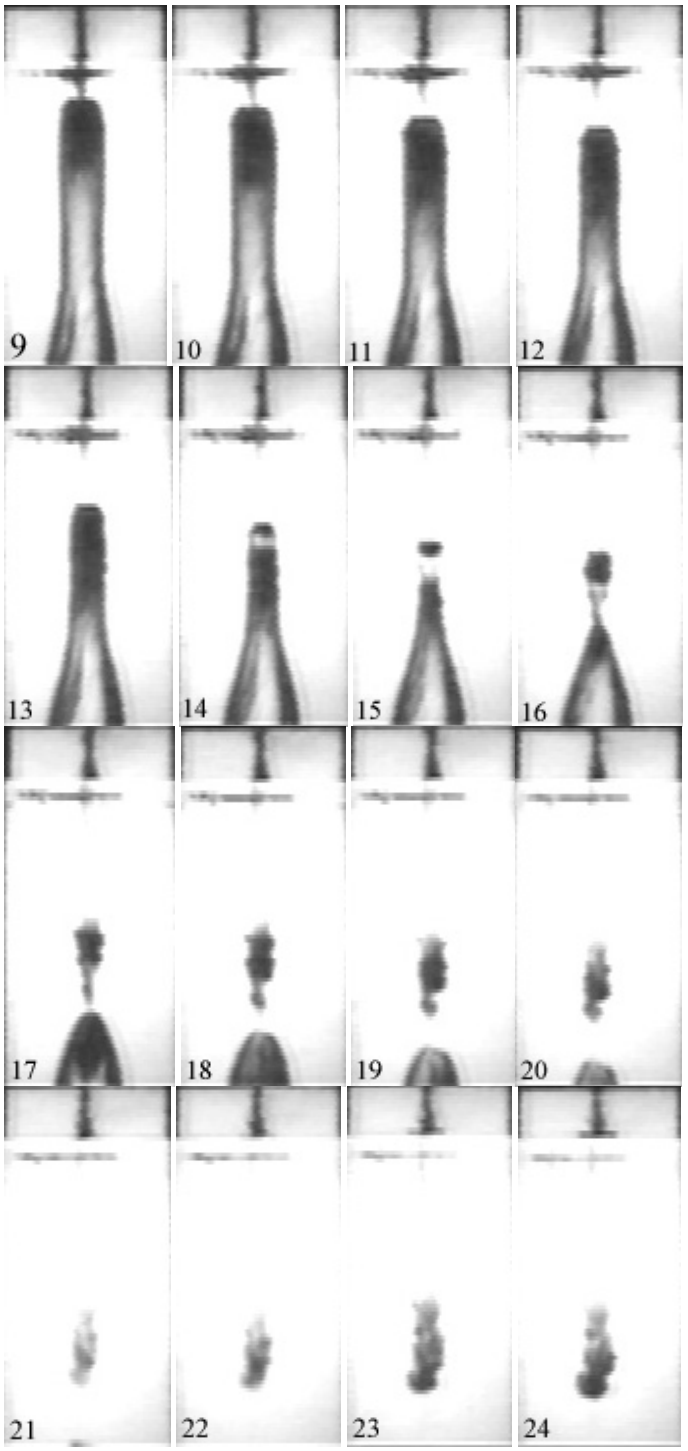

Figure 7: High-speed photographs of a three-dimensional supercavitation. The time between successive images is 0.5 ms. The height of each picture is 400 mm

$$V = 352\exp(-1.2Z), m/s \qquad (7)$$

where Z is in meter. Then it is estimated that the time in Fig. 7(1) is about 0.23 ms after water entry.

In Fig. 7(2), the water surface has been sealed. An upward splash in air and a downward jet in the cavity are visible. Their travelling distances from the surface are almost same. The splash velocity reaches $U_s \approx 83.58$ m/s that is in

agreement with the previous measurement in Sec. 3.1. The velocity of pulling the cavity away from the water surface U_p from Fig. 7(5) to Fig. 7(8) is 11.94 m/s while it is 17.91 m/s from Fig. 7(9) to Fig. 7(12).

One significant feature is that from Fig. 7(3), the lower part of the cavity is bent to the left and the cavity is no longer axisymmetric. Following the bending, the cavity's lower part quickly expands and its diameter becomes larger than that of the upper part. Another feature is that when the cavity's upper end breaks up to form a discrete bubble (Figs. 14-16), the bubble starts to collapses and rebounds independently (Figs. 17-24). In this case, the helical bubble does not appear instead the supercavity begins to collapse in Fig. 7(17) because a thick down jet has been formed in the cavity.

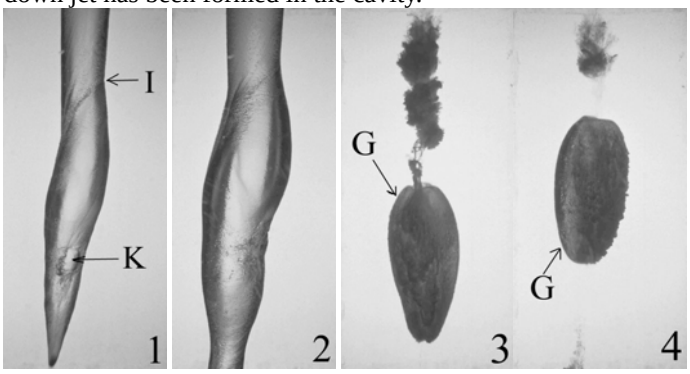

Figure 8: Single-shot photographs of three-dimensional supercavities and grain-like bubbles. The height of each picture is 400 mm. The top of the pictures is at 70 mm water depth

In order to investigate the mechanism of the formation of three-dimensional supercavity (see Fig. 7.), experiments have been carried out at a greater water depth. The results are given in Fig. 8. From Figs. 8(1) and 8(2), it can be understood that the cavity bending is caused by the trajectory deflection of the projectile. The deflection position is marked as I in Fig. 8(1). After the deflection occurs, the projectile start to rotate and this rotation exert its energy to the cavity wall [19] to bring about a sudden expansion of the cavity. This is why the cavity diameters at the bottom of the pictures in Figs. 7(8)-(16) are so large as compared with those in Fig.4. Consequently, the supercavity is twisted by the projectile's rotation. As a result, the upper and lower parts of the cavity are pinched off to form a grain-like bubble G shown in Figs. 8(3) and 8(4). It is clearly seen that the non-equilibrium condensing gas-liquid two-phase flow appears in the grain bubble. The rotating projectile often penetrates a hole on the cavity wall (see mark K in Fig. 8(1).). However, from the observed cavity shape shown in Figs. 8(1) and 8(2), it is known that the cavity is capable of mending the hole automatically by itself. Therefore, the supercavity must be in a thermodynamic state of highly non-equilibrium because only a great entropy potential can drive such a recovery process.

3.3 Deep Seal and Pinch-off

In order to investigate the mechanism of the grain bubble formation, high-speed photography has been conducted to observe deep seal and pinch-off processes which occur at positions above and below the grain bubble. This object is achieved by increasing the water depth. Deep seal (deep closure) means that the cavity closure occurs at a water depth, which is usually caused by pinch-off or necking of the cavity.

The three-dimensional supercavity shown in Fig. 9(a) is similar to that in Fig. 8(2). The energy transformation from the projectile to the cavity has caused a large diameter a gasbag-like cavity. At this time, the gasbag is still connected with the upper post supercavity as well as with the lower part new supercavity which is being fast pulled downwards by the projectile. Cavity pinch-off just occurs at these two connecting points. Figures 9(b)-(c) show that the upper pinch-off and deep seal are completed. The lower pinch-off is not seen in the figures because it is beyond the observation scope but the process is given in another experiment shown in Fig. 10. After deep seals have done, the separated helical bubble and grain bubble form and begin their individual cavitation processes through Figs. 9(d)-(h).

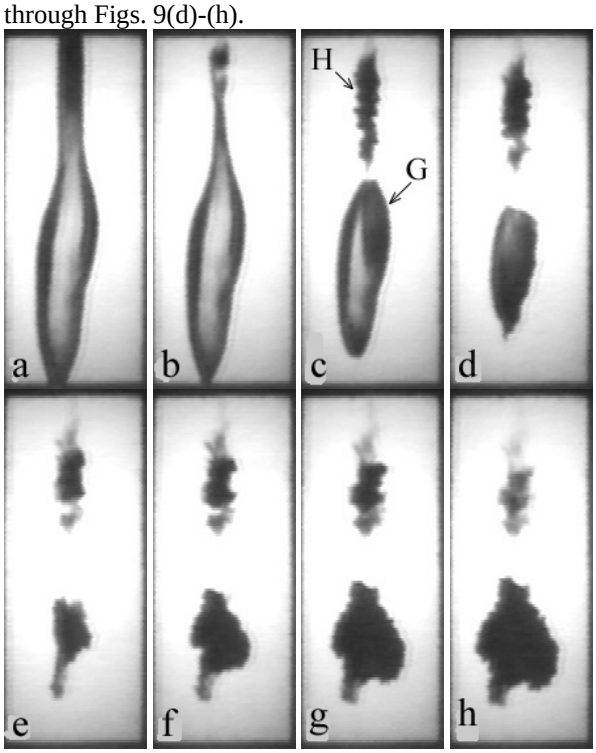

Figure 9: High-speed photographs of deep seal of supercavity at upper position. The ineterframe time is 1 ms. H and G are helical bubble and grain bubble respectively. The top of the pictures is at 100 mm water depth

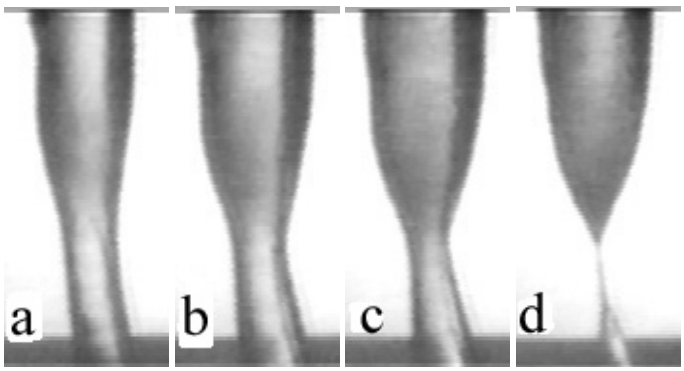

Figure 10: High-speed photographs of deep seal of supercavity at lower position. The interframe time is 1.5 ms

3.4 Surface Seal and Splash

It is very important to describe correctly the process of surface seal in water entry study. To achieve this task, high-speed photography of close views is performed, that is, the camera is moved more closer to the water tank. Figure 11 shows the close bird view of the formation of the splash. It is seen that at the beginning, the splash moves up vertically (Figs. 11(1)-(2)). However, due to the effects of gravity and air drag, the upper part of the splash decelerates and it collides with the following lower part of splash. Then horizontally moving sprays are formed (Figs. 11(4)-(8)).

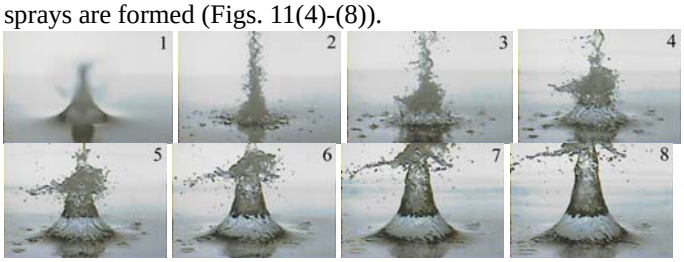

Figure 11: Bird view of the formation of splash. Interframe time is 1 ms

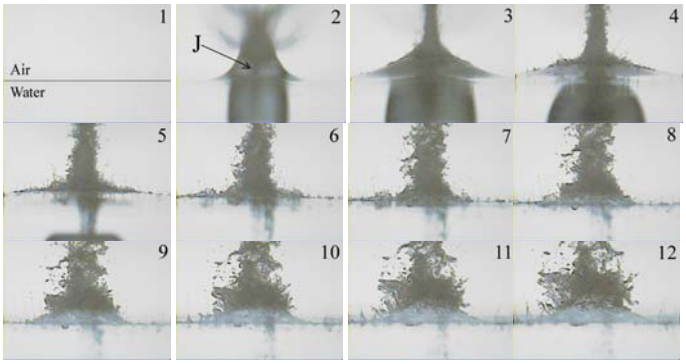

Figure 12: Close view of the formation of surface seal and down jet. Interframe time is 1 ms. The water level is elevated by the upwards splash in Figs. 12(3)-(5). The water level is pulled back again in Figs. 12(6)-(8) following the cavity pulling away process. Figures 12(9)-(12) show the water level becomes stable

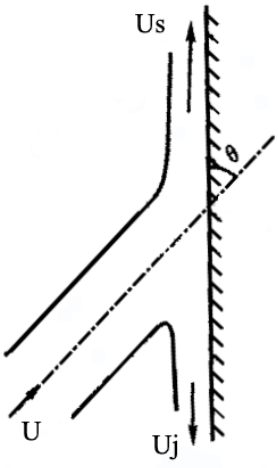

Figure 13: Theoretical model of the formation of splash and down jet

Figure 12 shows the close view of the formation of the surface seal and the down jet. Figure 12(1) is the sequence just before water entry. Figure 12(2) is the sequence when surface seal just occurs. The striking phenomenon is that a thin down jet (see mark J in Fig. 12(2).) forms simultaneously with the formation of the upward splash. The starting position for the jet formation is just the position of water crown collision, which is above the water surface.

In accordance with the experimental results, a theoretical model of describing the formation of splash and down jet is presented in Fig. 13. The axisymmetric splash flow is simplified as a plan problem, that is, a jet of water crown with velocity U impacts on a rigid wall with an inclination angle θ. The impact causes a splash jet with velocity U_s and a down jet with velocity U_j. For incompressible flow, from Bernoulli and continuum equations [20], it is well known that

$$U_s = U_j = U \tag{8}$$

$$\cos\vartheta = \frac{A_s - A_j}{A} \tag{9}$$

where A, A_s and A_j are the widths of water crown jet, splash and down jet respectively.

Equation (8) indicates that the splash velocity is equal to the down jet velocity. This is in a good agreement with the experimental data obtained in Secs. 3.1 and 3.2. On the other hand, since the down jet is very thin, that is, $A_j << A_s$. From Eq. (9), it is known that at the moment of surface seal, the water crown is nearly vertical ($\theta \sim 0$). The experiments presented in Figs. 5, 7, 11 and 12 all prove that this conclusion is correct.

4 CONCLUSIONS

We have examined the key factors of water entry problem such as surface seal, deep seal, splash, down jet and cavity pulling away from water surface, etc. The axisymmetric and three-dimensional supercavitations and the consequent helical bubble, gasbag as well as grain bubble are all studied. It is found that the axisymmetric and three-dimensional supercavities appear randomly. The current work has extended our previous understanding to water entry and supercavitation [15,16].

The comparison of our experimental data with the Logvinovish's theoretical model shows that the discrepancy is obvious. The cavity length L_c/D_n and maximum diameter D_c/D_n in the experiment are 75.61 and 9.50 respectively whereas they are 693.80 and 11.07 respectively predicted from Eqs. (1)-(3). The cavity maximum diameters of experiment and theory are in a good agreement but the cavity lengths are greatly different. The reasons for this are not clear yet. Even considering the variations in drag coefficient and cavitation number, the difference can not be compensated also. Basically, the Logvinivich's theory is suitable to describe a slender elliptical supercavity [8-10]. With the presence of a water surface, a supercavity is unlikely to develop into an elliptical shape that is symmetric about the position x of D_c/D_n. At deeper water depth, although the influence of water surface is far away, the deep seal and the increase of cavitation number will restrain the development of a supercavity. Therefore, the Logvinovich's

model may not best describe the supercavity in water entry or water exit.

The present experiment and theoretical analysis on the formation of splash and down jet reveal that they form simultaneously and have same velocities. The splash discussed here is at a later time when surface seal almost or just occurs. The splash formation at the early stage of water entry [21] is not applicable to this case. Furthermore, the surface seal is completed by the inwards collision of a nearly vertical water crown. The mechanism is related to the shape of cylindrical type projectile since the splash shape depends on the after-body shape [16]. The research on small ball water entry by Aristoff and Bush [3] indicates that during surface seal, the inclination angle of water crown jet θ can be around 40°.

It has been clarified that the grain bubble is primarily caused by the trajectory deflection of the underwater projectile. Truscott and Techet [3] demonstrate that spinning of solid ball can cause a curved underwater ball trajectory. However, in our case, the velocity of circumferential spinning of the projectile is only about 3% of the vertical impact velocity [18] so that it is impossible for the circumferential spinning to result in the trajectory deflection. The most possible reason for the deflection is the slamming between the solid body and the cavity wall, which has been indicated by Savchenko [10] and Rand et al. [22]. Of course, unsteadiness and turbulence of the flow field may add extra influences on the deflection.

ACKNOWLEDGMENTS

This work was supported by the Japan Society for the Promotion of Science, Tokyo, under a Grant-in-Aid for Scientific Research (Grant No. 12650162), and by Science Foundation of Zhejiang Sci-Tech University (ZSTU), China, under Grant No. 111331A3252357. The support from the National Natural Science Foundation of China is also thanked.

REFERENCES

[1] Chen, Y. and Lu, C. J. 2008, "A Homogenous Equilibrium Model Based Numerical Code for Cavitation Flows and Evaluation by Computation Case," *J. Hydrodynamics Ser. B*, 20(2), 186-194.

[2] Cao, W., Wang, C., Wei, Y. J. and Zou, Z. Z. 2006, "High-Speed Projectile Experimental Investigations on the Characteristics of Natural Supercavitation (in Chinese)," *Engineering Mechanics*, 23(12), 175-179.

[3] Aristoff, J. M. and Bush, J. W. M. 2009, "Water Entry of Small Hydrophobic Spheres" *J. Fluid Mech.*, 619, 45-78.

[4] Truscott, T. T. and Techet, A. H. 2009, "Water Entry of Spinning Spheres" *J. Fluid Mech.*, (in press).

[5] Hrubes, J. D. 2001, "High-Speed Imaging of Supercavitating Underwater Projectile," *Experiments in Fluids*, 30(1), 57-64.

[6] Klomfass, A. and Salk, M. 2005, "Numerical Analysis of the Supercavitating Supersonic Flow about Blunt Bodies," *Proc. 25th Int. Symp. on Shock Waves*, Paper No. 1232-1a, pp.997-1002, July 17-22, Bangalore, India.

[7] Neaves, M. D. and Edwards, J. R. 2006, "All-Speed Time-Accurate Underwater Projectile Calculations Using a Preconditioning Algorithm," *Trans ASME, J. of Fluids Engineering*, 128, 284-296.

[8] Savchenko, Y. N. 2001, "Experimental Investigation of Supercavitating Motion of Bodies," *RTO AVT Lecturer Series EN-010-04*, von Karman Institute (VKI), Brussels, Belgium.

[9] Savchenko, Y. N. 2001, "Artificial Supercavitation: Physics and Calculation," *RTO AVT Lecturer Series EN-010-11*, von Karman Institute (VKI), Brussels, Belgium.

[10] Savchenko, Y.N. 2001, "Control of Supercavitation Flow and Stability of Supercavitating Motion of Bodies," *RTO AVT Lecturer Series EN-010-14*, von Karman Institute (VKI), Brussels, Belgium.

[11] Vlasenko, Y. D. 1998, "Experimental Investigations of High-Speed Unsteady Supercavitating Flows," *Proc. 3rd Int. Symp. on Cavitation*, Vol.2 pp.39-44, Grenoble, France.

[12] Kirschner, I. N. 2001, "Results of Selected Experiments Involving Supercaviting Flows," *RTO AVT Lecturer Series EN-010-15*, von Karman Institute (VKI), Brussels, Belgium.

[13] Shi, H. H. and Takami, T. 2001, "Hydrodynamic Behavior of an Underwater Moving Body after Water Entry," *Acta Mechanica Sinica*, 17(1), 35-44.

[14] Shi, H. H. and Kume, M. 2001, "An Experimental Research on the Flow Field of Water Entry by Pressure Measurements," *Physics of Fluids*, 13(1), 347-349.

[15] Shi, H. H. and Kume, M. 2004, "Underwater Acoustics and Cavitating Flow of Water Entry," *Acta Mechanica Sinica*, 20(4), 374-382.

[16] Shi, H. H., Itoh, M. and Takami, T. 2001, "Optical Observation of the Supercavitation Induced by High-Speed Water Entry," *Trans. ASME, J. of Fluids Engineering*, 122(4), 806-810.

[17] Knapp, R. T., Daily, J. W. and Hammitt, F. G. 1970, *Cavitation*, McGraw-Hill, New York.

[18] Shi, H. H. and Takami, T. 2001, "Some Progress in the Study of the Water Entry Phemonenon," *Experiments in Fluids*, 30, 475-477.

[19] Lee, M., Longoria, R. G. and Wilson, D. E. 1997, "Cavity Dynamics in High-Speed Water Entry," *Physics of Fluids*, 9, 540-550.

[20] Hughes, W. F. and Brighton, J. A. 1999, *Theory and Problems of Fluid Dynamics*, McGraw-Hill, New York.

[21] Shi, H. H. 1997, "Fast Water Entry of Blunt Solid Projectile," *Proc. 74th JSME Spring Annual Meeting*, Tokyo, Vol. VI, pp.1-4.

[22] Rand, R., Pratap, R., Ramani, D., Cipolla, J. and Krischner, I. 1997, "Impact Dynamics of a Supercavitating Underwater Projectile," *Proc. 1997 ASME Design Engineering Technical Conference*, DETC97/VIB-3929, Sacramento, California, September 14-17.